

Monte Carlo Study Based on a Real Coordinate System for Tangentially Injected High-Energy Particles in the Large Helical Device

Ryosuke SEKI^{a)}, Yutaka MATSUMOTO, Yasuhiro SUZUKI¹⁾, Kiyomasa WATANABE¹⁾, Kiyotaka HAMAMATSU²⁾ and Masafumi ITAGAKI

Graduate School of Engineering, Hokkaido University, Sapporo 060-8628, Japan

¹⁾*National Institute for Fusion Science, Toki 509-5292, Japan*

²⁾*Japan Atomic Energy Agency, Naka 311-0193, Japan*

(Received 18 September 2009 / Accepted 31 May 2010)

A new Monte Carlo code based on particle tracing using real coordinates has been developed to properly treat the re-entering particles that repeatedly pass in and out of the last closed flux surface (LCFS). The particle loss due to the charge-exchange reaction has also been taken into account in this code. We apply this new code to the analysis of high-energy particles produced by tangential neutral beams (NBs) of the large helical device (LHD). It is confirmed that reasonable solutions of distribution functions are obtained for particles produced by the tangential-NBs. It is also confirmed that the effect of the particle orbit and the charge-exchange loss on the distribution function is properly included. The shapes of the distribution functions of particles, produced by the tangential-NBs in two temperature cases (1 keV and 0.1 keV), are the same. It is found that the re-entering particles play an important role in the analyses of the distribution function of particles produced by the NBs.

© 2010 The Japan Society of Plasma Science and Nuclear Fusion Research

Keywords: Monte Carlo simulation, LHD, re-entering particle, tangential neutral beam, charge-exchange loss

DOI: 10.1585/pfr.5.027

1. Introduction

Three tangential neutral beam (NB) injectors and a perpendicular-NB injector have been installed on the large helical device (LHD) [1]. A volume-averaged beta, $\langle\beta\rangle$, reached 5% in recent LHD experiments using these NBs [2]. In the high-beta plasma of the LHD, the typical operational magnetic field strength is low, and the typical high-beta discharges are operated under the relatively low density because the so-called density limit decreases as the magnetic field strength decreases [3]. The beta value achieved increases with a decrease in magnetic field strength. On the other hand, the increase in the stored energy of the high-energy particles due to the decrease in operational density is superior to the degradation of confinement of the high-energy particles caused by the decrease in magnetic field strength. The ratio of the beam pressure to the total plasma pressure is relatively high. Here, the beam pressure is the pressure caused by the high-energy particles produced by the NBs. Because it has been pointed out that the beam pressure and/or the pressure anisotropy significantly affects the properties of MHD equilibrium and stability [4–6], it is important to identify the beam-pressure in the total plasma pressure.

To calculate the beam pressure, we need to know the

distribution function of the high-energy particles produced by the NBs. The distribution function can be obtained by a Monte Carlo simulation based on high-energy particle tracing. The conventional Monte Carlo simulation studies for the LHD have been performed with the use of the Boozer coordinates [7, 8]. On the LHD high beta study based on the above method, the particle-loss boundary is set on the last closed flux surface (LCFS) in the particle tracing. Therefore, once having passed out of the LCFS, the particles are regarded as lost particles. As a result, the particle loss is overestimated in such analyses.

On the other hand, the authors have performed particle orbit analyses using the real coordinates, where the particle-loss boundary is set on the vacuum vessel wall [9]. In these analyses, it has been shown that the re-entering particles [10, 11] that repeatedly pass in and out of the LCFS, exist in both the vacuum magnetic field and the finite-beta plasma. It has been pointed out that the role of the re-entering particles in the high-energy particle behavior in a finite-beta plasma and/or a low-strength magnetic field is more important than that in the vacuum magnetic field.

In this paper, we develop a new Monte Carlo code based on particle tracing with the use of real coordinates. As a code based on a similar concept, the orbit-following Monte Carlo (OFMC) code [12] was developed for JT-60U experimental analyses. In the developed code, as the

author's e-mail: seki.ryosuke@lhd.nifs.ac.jp

^{a)} present address: National Institute for Fusion Science, Toki 509-5292, Japan

particle-loss boundary is set on the vacuum vessel wall the re-entering particles can be traced properly. The re-entering particles repeatedly pass through the outer region of the LCFS, where the neutral particle density is higher than that in the core. Consequently, the re-entering particles might be lost because of the charge-exchange reaction with the neutral particles. Considering this fact, the particle loss due to the charge-exchange reaction is included in the developed code.

We apply this code to the high-energy particles produced by the tangential-NBs of the LHD in the vacuum magnetic field. The difference in the distribution function caused by the change in temperature of back ground plasma is also investigated. We also study the effects of the charge-exchange reaction as well as the re-entering particles on the distribution functions.

This paper is organized as follows. The outline of the developed Monte Carlo code is summarized in Sec. 2. The application results of the Monte Carlo code to the high-energy particles produced by the tangential-NBs are presented in Sec. 3. The conclusion is presented in Sec. 4.

2. Developed Monte Carlo Code

2.1 Outline to calculate the distribution function

To analyze the distribution function of the high-energy particles that are peculiar to the LHD as a helical device, we have developed a new Monte Carlo code. The outline of this code is explained as follows.

This code calculates the steady-state solution of the drift-kinetic equation through particle tracing. To trace the high-energy particles, guiding-center equations are numerically solved in real coordinates. Coulomb collision is taken into account using the Monte Carlo collision operator [13] described in Sec. 2.2. The particle-loss boundary is set on the vacuum vessel wall instead of the LCFS to trace the re-entering particles properly. In this paper, the particle reaching the vacuum vessel wall or making the charge-exchange reaction is regarded as a lost particle. The treatment of the charge-exchange loss is explained in Sec. 2.3. We use the 6th-order Runge-Kutta formulas [14] and the 3D higher order spline function [15] in the particle tracing calculation.

Each Monte Carlo particle with a weight $W = S_0/N_{\text{cal}}^{\text{total}}$ is traced until it is either thermalized or lost. Here, $N_{\text{cal}}^{\text{total}}$ is the total number of traced Monte Carlo particles and $S_0 = P_{\text{NB}}/E_{\text{NB}}$ denotes the number of high-energy charged particles produced by NBs per unit time. P_{NB} is the injected power by NBs and E_{NB} the energy of a high-energy charged particle produced by NB. Note that the number distribution of the high-energy particle produced by NB shows $N_{\text{birth}}(r_{\text{initial}}) = W \times N_{\text{cal}}(r_{\text{initial}})$, where r_{initial} is the position of an initial point of a Monte Carlo particle and N_{cal} is the number of Monte Carlo particle traced from each initial points, $N_{\text{cal}}^{\text{total}} = \sum N_{\text{cal}}(r_{\text{initial}})$. In

this code, the thermalized particle is defined as the particle whose velocity has become less than three times v_{Tb} because of the Coulomb collision. Here, $v_{\text{Tb}} (= \sqrt{T_{\text{b}}/m_{\text{b}}})$ is the thermal velocity of the back ground particle. As a result of particle tracing, we obtain the time $\Delta t(r, \theta, \varphi, v, \chi)$ that a Monte Carlo particle spends in a small volume in phase space, as $\Delta V(r, \theta, \varphi, v, \chi) = R_{\text{ax}} r \Delta r \Delta \theta \Delta \varphi 2\pi v^2 \sin(\chi) \Delta v \Delta \chi$. Then, the distribution function is approximately given by

$$f(r, \theta, \varphi, v, \chi) = \frac{1}{\Delta V(r, \theta, \varphi, v, \chi)} \sum_{i=1}^{N_{\text{cal}}^{\text{total}}} W_i \times \Delta t_i(r, \theta, \varphi, v, \chi), \quad (1)$$

where r denotes the minor radius, θ and φ are the poloidal and toroidal angles, respectively, and χ the pitch angle. Here, R_{ax} is the major radius at the magnetic axis. The pressure and some other quantities can be calculated from the obtained distribution function.

2.2 Collision operator

The following Coulomb collision operator [13] is introduced in the developed code. In this model, the test particle is assumed to continuously collide with the back-ground Maxwellian plasma. Based on mean values and mean square deviations of the velocity variation due to collision, the velocity variation (Δv_v , Δv_χ , Δv_η) is added to the velocity of the test particle after each small time step δt . Here, χ is the pitch angle, while η corresponds to the gyro-phase.

A test particle (subscript ‘‘t’’) collides with back-ground particles (subscript ‘‘b’’). Provided that the back-ground particles have a Maxwellian velocity distribution with temperature T_{b} , the mean values and mean square deviations of the test particle during δt are given by [16]

$$\langle (\Delta v_v^{t/b})^2 \rangle = \frac{\Gamma^{t/b}}{2v} \left[\frac{\text{erf}(u)}{u^2} - \frac{\text{erf}'(u)}{u} \right] 2\delta t, \quad (2)$$

$$\langle \Delta v_v^{t/b} \rangle = - \left(1 + \frac{m_t}{m_b} \right) \frac{\Gamma^{t/b}}{v^2} (\text{erf}(u) - u \text{erf}'(u)) \delta t, \quad (3)$$

$$\langle (\Delta v_\chi^{t/b})^2 \rangle = \langle (\Delta v_\eta^{t/b})^2 \rangle = \frac{\Gamma^{t/b}}{4v} \left[\left(2 - \frac{1}{u^2} \right) \text{erf}(u) + \frac{\text{erf}'(u)}{u} \right] 2\delta t, \quad (4)$$

and

$$\langle \Delta v_\chi^{t/b} \rangle = \langle \Delta v_\eta^{t/b} \rangle = 0, \quad (5)$$

where $u = v/(\sqrt{2}v_{\text{Tb}})$. Here, $\text{erf}(u) = (2/\sqrt{\pi}) \int_0^u \exp(-x^2) dx$ is the error function and $\text{erf}'(u) = (2/\sqrt{\pi}) \exp(-u^2)$ the differentiated error function. $\Gamma^{t/b} = n_b q_t^2 q_b^2 \ln \Lambda^{t/b} / (4\pi \epsilon_0^2 m_t^2)$, where q_a , m_a and n_a are the electric charge, mass, and density of species ‘‘a’’, respectively. ϵ_0 is the dielectric constant in vacuum. The Coulomb logarithm $\ln \Lambda^{t/b}$ is given in the NRL Plasma Formulary [17].

A set of (Δv_v , Δv_χ , Δv_η) is computed using normal random numbers with Eqs. (2)-(5). As a result, the velocity

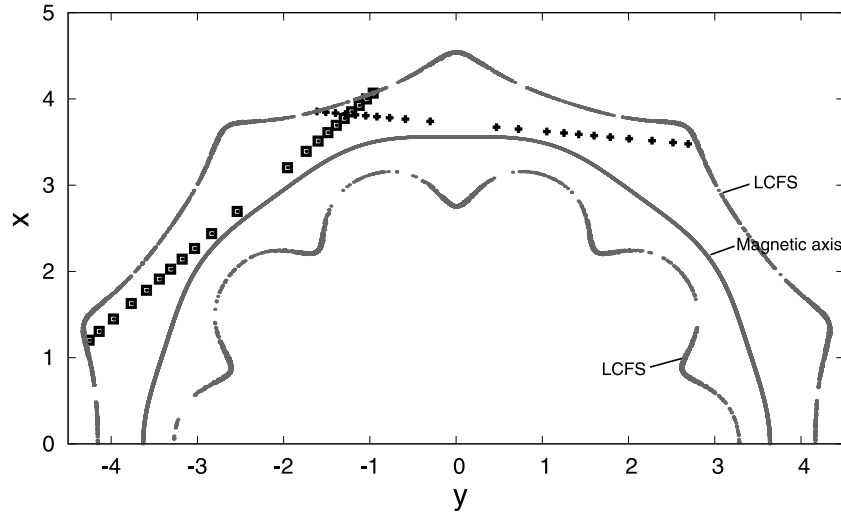


Fig. 1 Initial points of Monte Carlo particles on the equatorial plane in the LHD. Square marks are the initial points in counter-NB case and crosses are the initial points in co-NB case.

$(v_{\parallel}, v_{\perp})$ changes to

$$v'_{\parallel} = v_{\parallel} + \Delta v_v^{t/b} \frac{v_{\parallel}}{v} - \Delta v_{\chi}^{t/b} \frac{v_{\perp}}{v}, \quad (6)$$

and

$$v'_{\perp} = \left[\left(v_{\perp} + \Delta v_v^{t/b} \frac{v_{\perp}}{v} + \Delta v_{\chi}^{t/b} \frac{v_{\parallel}}{v} \right)^2 + \left(\Delta v_{\eta}^{t/b} \right)^2 \right]^{\frac{1}{2}}, \quad (7)$$

during δt by collisions, respectively.

2.3 Charge-exchange loss

As mentioned above, in order to investigate the effect of the re-entering particle on the distribution function, it is important to deal with the charge-exchange loss. In this paper, the charge-exchange reaction is modeled as follows [18].

The probability of the charge-exchange reaction during δt is expressed as $n_n \langle \sigma \rangle_{cx} v \delta t$ when a high-energy charged particle passes through the space with neutral particle density n_n . Here, $\langle \sigma \rangle_{cx}$ is the reaction cross-section for charge-exchange reaction. The probability is integrated along the charged particle orbit as $I = \int n_n \langle \sigma \rangle_{cx} v dt$, until $I = \ln(1/\alpha)$. In other words, the high-energy charged particle is lost because of the charge-exchange reaction when $I = \ln(1/\alpha)$, where α is a random number such that $0 < \alpha < 1$. In this paper, it is assumed that neutral particles exist only outside the LCFS with $n_n = \text{const}$. Therefore, the charge-exchange also reacts only outside the LCFS.

3. Computational Results Obtained by the Developed Code

3.1 Calculation conditions

We apply the new Monte Carlo code to the high-energy particles produced by the tangential-NBs (BL-1 and BL-2) in the LHD. Note that the injecting direction of BL-1 is opposite to that of BL-2. Although each NB injector

has two beam lines, the initial points of the Monte Carlo particles are assumed to be set on a line between these two beam lines for simplicity. As shown in Fig. 1, we set 21 initial points on the line inside the LCFS in each NB [19]. The initial points expressed in the normalized minor radius, ρ , are evenly spaced apart ($\Delta \rho \approx 0.04$). Here, $\rho = \sqrt{\psi/\psi_{\text{LCFS}}}$, ψ_{LCFS} is the toroidal magnetic flux at the LCFS. The number of Monte Carlo particles traced from each initial point is 1,000 and W of each Monte Carlo particle is the same for simplicity. As a result, the number of high-energy particles produced by the NB is uniform in terms of ρ and the birth profile of the high-energy particles produced by the NB is in inverse proportion to ρ^2 . The initial energy (E_0) of the particles is assumed to be 180 keV, which corresponds to a typical value of the operational beam energy. The direction of the initial velocity of the particle corresponds to the direction of the beam line. The other conditions used in this paper are shown in Table 1. The background plasma is assumed to consist of a proton and an electron, and impurity ions are ignored. The temperature and density of the background plasma are assumed to be constant throughout the region inside the vacuum vessel wall.

3.2 Distribution function of particles

In each component of the phase space (ρ, v, χ) , the distribution function is given by

$$F_v(v) \equiv \iiint f(\rho, \theta, \phi, v, \chi) R_{ax} \rho \sin(\chi) d\rho d\theta d\phi d\chi, \quad (8)$$

$$F_{\rho}(\rho) \equiv \iiint f(\rho, \theta, \phi, v, \chi) 2\pi v^2 \sin(\chi) d\theta d\phi dv d\chi, \quad (9)$$

and

$$F_{\chi}(\chi) \equiv \iiint f(\rho, \theta, \phi, v, \chi) R_{ax} \rho 2\pi v^2 d\theta d\phi dv, \quad (10)$$

Table 1 Calculation conditions

Magnetic field			
β			0% (vacuum)
Field strength on the magnetic axis (B_{ax})			3 T
Major radius on the magnetic axis (R_{ax})			3.6 m
Background			
species	hydrogen		
ion	temperature	T_{bi}	1.0 keV
	density	n_{bi}	10^{20} m^{-3}
electron	temperature	T_{be}	1.0 keV
	density	n_{be}	10^{20} m^{-3}
Neutral Beams			
injected power	counter		1 MW
	co		1 MW

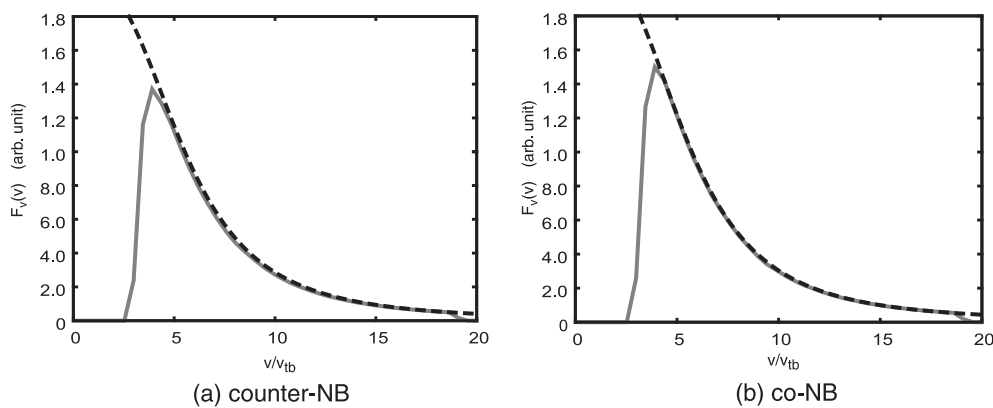


Fig. 2 Distribution functions in the velocity space are shown by the solid lines: (a) shows counter-NB case and (b) co-NB case. The analytical steady-state solution of the Fokker-Planck equation is drawn as reference (dashed line). Note that $F_v(v)$ in the two cases is shown in the same unit. Calculation conditions are shown in Table 1.

respectively. Note that here, owing to the above definition, $F_\rho(\rho)$ corresponds to the density profile.

The solid line in Fig. 2 shows the $F_v(v)$ calculated by Eq. (8). It should be noted that the units are the same in Figs. 2(a) and (b). In Fig. 2, the $F_v(v)$ (solid line) is in agreement with the analytical steady-state solution of the Fokker-Planck equation (dashed line) [20]. This result implies that the energy-relaxation process of the high-energy particles is successfully calculated. The peak value of $F_v(v)$ in the case of counter-NB is slightly smaller than that in the case of co-NB. This difference is attributed to the difference in the number of lost particles in the two injection cases. Although there are few lost particles traced from $\rho \approx 1.0$ in the case of co-NB, most of the particles traced from $\rho \approx 1.0$ are lost in the case of counter-NB.

Figure 3 shows the $F_\rho(\rho)$ cause using Eq. (9). In Fig. 3, the solid and dashed lines are the $F_\rho(\rho)$ calculated with and without tracing particles, respectively. In counter-NB case (Fig. 3 (a)), clear differences between the two $F_\rho(\rho)$ s with and without tracing particles in $\rho < 0.3$ and $\rho > 0.8$ can be seen. These differences are attributed

to the effect of the particle orbit on $F_\rho(\rho)$. The difference in $\rho < 0.3$ shows that the particle produced by counter-NB tends to move in the outer region of the flux surface on which its initial point is set. The difference in $\rho > 0.8$ is due to the orbit loss. On the other hand, in $0.3 < \rho < 0.8$, $F_\rho(\rho)$ is almost the same as $F_\rho(\rho)$ calculated without tracing particles. Most of the particles produced by tangential-NBs are passing particles. Additionally, in the applied calculation condition, the deviation of each passing particle orbit from the flux surface is small and almost the same. Therefore, in $0.3 < \rho < 0.8$, the particle orbit has little effect on $F_\rho(\rho)$. Also in the case of counter-NB, there are clear differences between the two $F_\rho(\rho)$ s with and without tracing particles in $\rho < 0.3$ and $\rho > 0.8$ in co-NB case (Fig. 3 (b)). These differences in co-NB case are because particles produced by co-NB tend to move in the inner region of the flux surface on which their initial points are set.

Figure 4 shows the $F_\chi(\chi)$ calculated using Eq. (10). In counter-NB case (Fig. 4 (a)), $F_\chi(\chi)$ peaks only at $\chi \approx \pi$ and the half-width of $F_\chi(\chi)$ at the half-maximum is about

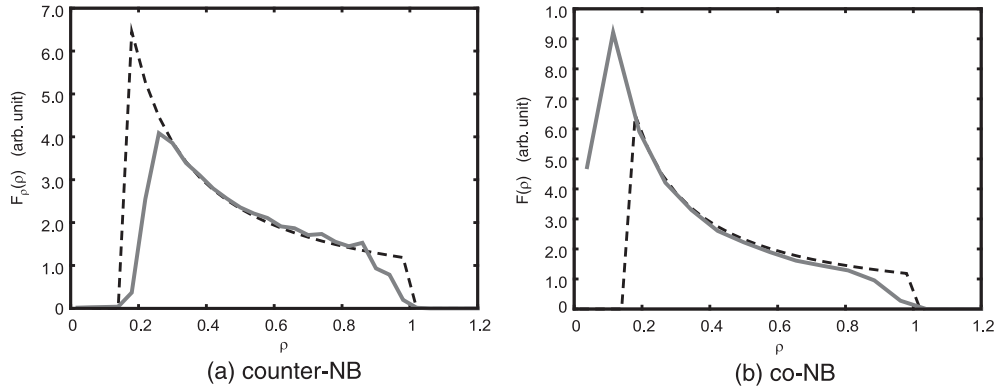


Fig. 3 Distribution functions in the ρ space are shown by the solid lines: (a) shows counter-NB case and (b) co-NB case. The distribution function calculated without tracing particles is shown as a reference (dashed line). Calculation conditions are shown in Table 1.

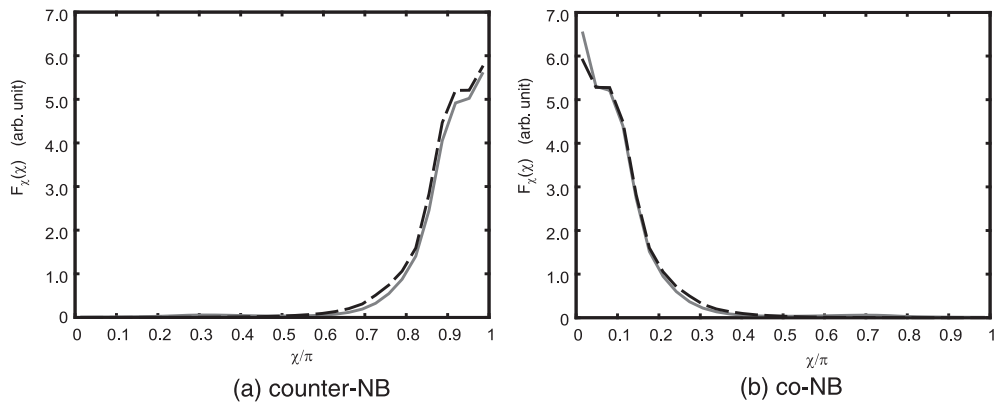


Fig. 4 Distribution functions in the χ space are shown by the solid lines: (a) shows counter-NB case and (b) co-NB case. The distribution function calculated without tracing particles is shown as a reference (dashed line). Calculation conditions are shown in Table 1.

0.2π . Additionally, in $\chi < 0.6\pi$, $F_\chi(\chi) \approx 0$. In contrast, in the case of co-NB, $F_\chi(\chi)$ has maximum value when $\chi \approx 0$ and $F_\chi(\chi) \approx 0$ in $\chi > 0.4\pi$. The half-width of $F_\chi(\chi)$ at the half-maximum is about 0.2π , which is the same as that in counter-NB case. These results imply that the influence of pitch-angle scattering on the distribution function is small.

3.3 Beam pressure estimated from obtained distribution functions

We estimate the beam pressure from the distribution functions obtained. The parallel and perpendicular beam pressures are given by

$$P_{\parallel}(\rho) \equiv 2 \iiint \int \frac{1}{2} m v^2 \cos^2(\chi) f(\rho, \theta, \phi, v, \chi) \times 2\pi v^2 \sin(\chi) d\theta d\phi dv d\chi, \quad (11)$$

and

$$P_{\perp}(\rho) \equiv \iiint \int \frac{1}{2} m v^2 \sin^2(\chi) f(\rho, \theta, \phi, v, \chi) \times 2\pi v^2 \sin(\chi) d\theta d\phi dv d\chi, \quad (12)$$

respectively. Figure 5 shows P_{\parallel} and P_{\perp} . Note that the injected power of NB is assumed to be 1 MW.

In Figs. 5 (a) and (b), there are clear differences between the two P_{\parallel} s with and without tracing particles in $\rho < 0.3$ and $\rho > 0.8$. Additionally, the shapes of P_{\parallel} are almost the same as those of $F_{\rho}(\rho)$, as shown in Fig. 3. In Figs. 5 (c) and (d), there also exist clear differences between the two P_{\perp} s with and without tracing particles in $0.3 < \rho < 0.8$. In other words, the particle orbit has an effect on P_{\perp} independent of ρ in the tangential-NB case. The scale of P_{\perp} is less than one twentieth of the scale of P_{\parallel} . In order to ascertain the validity of these results, we need to compare the new code results with the experimental results. We have a plan to analyze the distribution function of the NBs with the use of conditions much closer to those used in the actual LHD experiments.

3.4 Effect of back ground plasma on the distribution function

In order to investigate the effect of back ground temperature on the distribution function, we compare the distribution function in $T_b = 0.1$ keV with that of $T_b = 1$ keV. Figure 6 shows the distribution functions normalized by $W \times N_{\text{cal}} \times \langle \tau_{\text{rel}} \rangle$ in counter-NB case, where $\langle \tau_{\text{rel}} \rangle$ is the

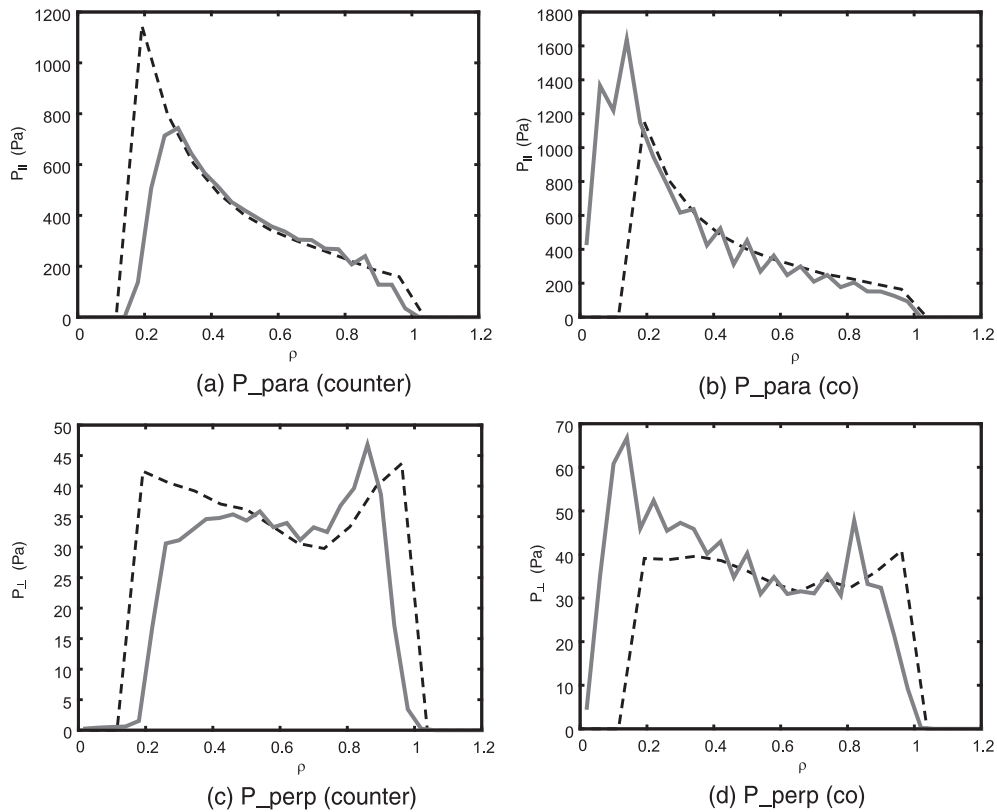


Fig. 5 Beam pressures (P_{\parallel} and P_{\perp}) obtained by the developed code are shown by the solid lines: (a) shows P_{\parallel} in counter-NB case. (b) shows P_{\parallel} in co-NB case, (c) shows P_{\perp} in counter-NB case and (d) shows P_{\perp} in co-NB case. The beam pressure calculated without tracing particles is shown for reference (dashed line). Calculation conditions are shown in Table 1.

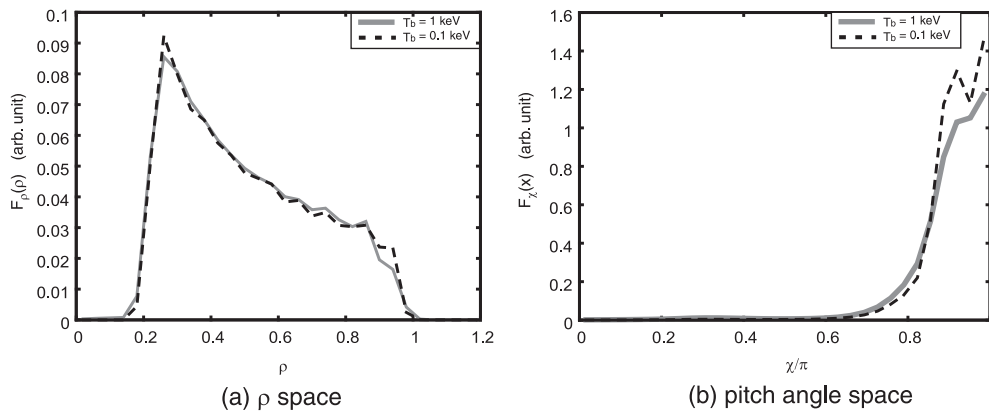


Fig. 6 Distribution functions of the particles produced by counter-NB in the $T_b = 1$ keV and $T_b = 0.1$ keV cases are shown by the solid and the dashed lines, respectively: (a) shows $F_{\rho}(\rho)$ and (b) shows $F_{\chi}(\chi)$. Calculation conditions are shown in Table 1.

average relaxation time of Monte Carlo particles.

In Fig. 6 (a), there is no significant difference in the shapes of $F_{\rho}(\rho)$ between the two T_b cases. Additionally, in Fig. 6 (b), the half-width of $F_{\chi}(\chi)$ at half-maximum in $T_b = 0.1$ keV is almost the same as that in the case where $T_b = 1$ keV. When the critical energy (E_c) is more than the energy of the particles (E), the effect of pitch-angle scattering is large. Because $E_c \approx 14.8$ keV ($T_b = 1$ keV) and $E_c \approx 1.48$ keV ($T_b = 0.1$ keV) in the conditions used,

$E_0 \gg E_c$. Additionally, during the calculation, the period in which $E > E_c$ is much longer than the period in which $E \leq E_c$. Therefore, pitch-angle scattering has little effect on the distribution function in the two T_b cases. As a result, the shapes of the distribution functions in the two T_b cases are almost the same.

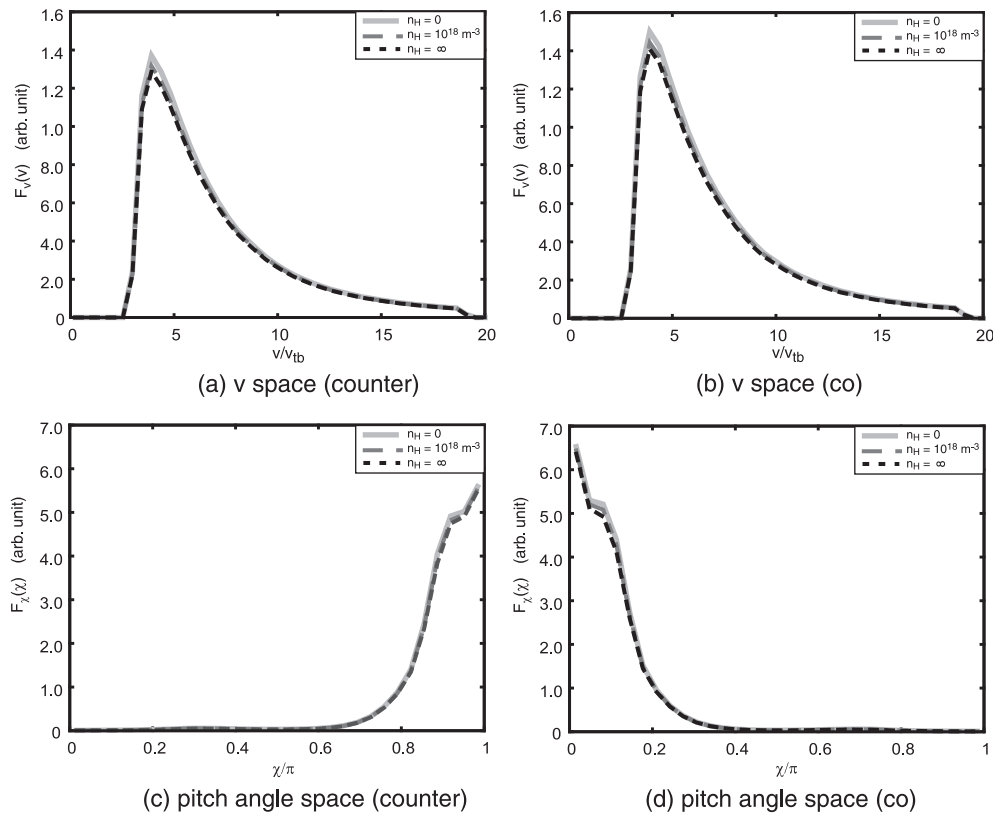


Fig. 7 Distribution functions in v and χ spaces considering the charge-exchange reaction for the cases with $n_H = 0$ (solid line), $n_H = 10^{18} \text{ m}^{-3}$ (dash-dotted line) and $n_H = \infty$ (dashed line): (a) shows $F_v(v)$ in counter-NB case, (b) $F_v(v)$ in co-NB case, (c) $F_\chi(\chi)$ in counter-NB case, and (d) $F_\chi(\chi)$ in co-NB case. Calculation conditions are shown in Table 1.

3.5 Effect of the charge-exchange loss on the distribution function

In this paper, we assume that the charge-exchange loss occurs only with hydrogen atoms and that the density of the hydrogen atoms (n_H) is uniform outside the LCFS and $n_H = 0$ inside the LCFS.

Figure 7 shows $F_v(v)$ and $F_\chi(\chi)$ in the $n_H = 0$, $n_H = 10^{18} \text{ m}^{-3}$, and $n_H = \infty$ cases. In Fig. 7, the solid line denotes the $n_H = 0$ case without charge-exchange loss. The dashed line represents the $n_H = \infty$ case, in which all the re-entering particles are regarded as lost particles. The dashed-dotted line denotes $n_H = 10^{18} \text{ m}^{-3}$ case. This value is estimated by the degree of vacuum obtained in the LHD experiments.

In Figs. 7 (a) and (b), there is no significant difference in $F_v(v)$ between the $n_H = 0$ and $n_H = \infty$ cases. Therefore, the charge-exchange reaction has a small effect on $F_v(v)$ of high-energy particles produced by the tangential-NB with $B_{ax} = 3 \text{ T}$. Similarly, in Figs. 7 (c) and (d), the charge-exchange loss hardly affects $F_\chi(\chi)$ of the high-energy particles produced by the tangential-NB.

Figure 8 shows $F_\rho(\rho)$ in the $n_H = 0$, $n_H = 10^{18} \text{ m}^{-3}$, and $n_H = \infty$ cases. The difference in $F_\rho(\rho)$ between $n_H = 0$ (solid line) and $n_H = 10^{18} \text{ m}^{-3}$ (dashed-dotted line) is remarkable only in $\rho \approx 1.0$. Therefore, in the case of tangential-NB with $B_{ax} = 3 \text{ T}$, the charge-exchange loss

has an effect on the distribution function in the vicinity of the LCFS. This is not only because most of the particles produced by the tangential-NB are passing particles, but also because the deviation of the passing particle orbit from the flux surface on which its initial point is set is relatively small when $B_{ax} = 3 \text{ T}$. Therefore, under the present calculation condition, only particles traced from the initial points near the LCFS are lost because of the charge-exchange reaction. In Fig. 8, there is also a clear difference in the distribution function between $n_H = 10^{18} \text{ m}^{-3}$ (dashed-dotted line) and $n_H = \infty$ (dashed line) in $\rho \sim 1$. This result implies that it is important to take the re-entering particles into account correctly in the analyses of the distribution function even in the case of tangential-NB with $B_{ax} = 3 \text{ T}$.

3.6 Distribution function in the finite-beta plasma of the LHD

As mentioned in Sec. 1, the role of the re-entering particles in the the high-energy particle behavior in the finite-beta plasma and/or the low-strength magnetic field may be more important than that in the vacuum magnetic field. The new Monte Carlo code is applied to the high-energy particles produced by the tangential-NBs in the finite-beta plasma of the LHD. The finite-beta equilibrium magnetic field ($\langle \beta \rangle = 2.7\%$, $B_{ax} = 0.5 \text{ T}$) used is calculated using the

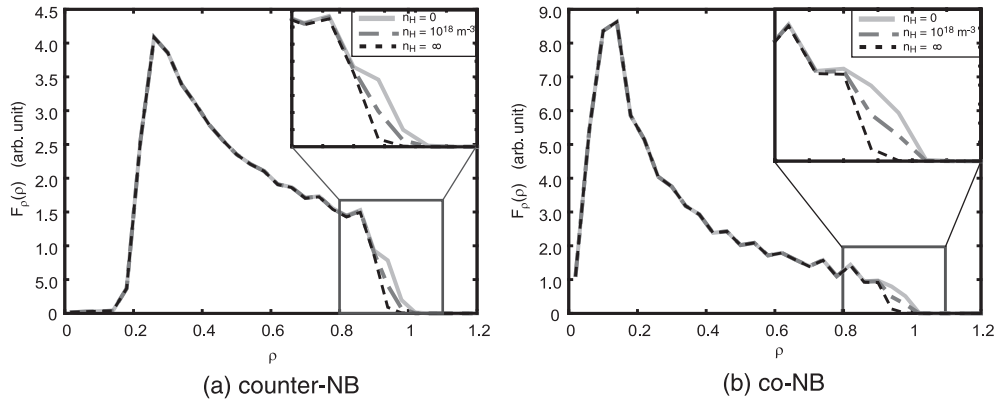


Fig. 8 Distribution functions in ρ spaces considering the charge-exchange reaction for the cases with $n_H = 0$ (solid line); $n_H = 10^{18} \text{ m}^{-3}$ (dash-dotted line) and $n_H = \infty$ (dashed line). (a) shows counter-NB case and (b) co-NB case. Calculation conditions are shown in Table 1.

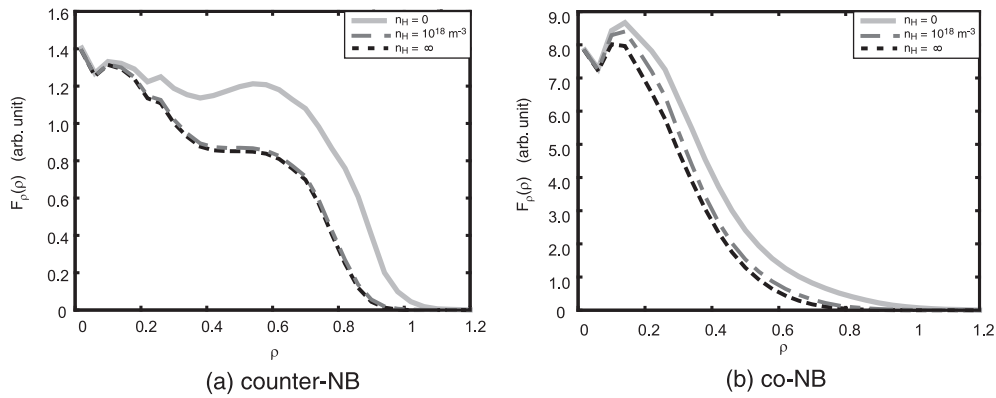


Fig. 9 Distribution functions in the finite-beta plasma of the LHD for the cases with $n_H = 0$ (solid line), $n_H = 10^{18} \text{ m}^{-3}$ (dash-dotted line), and $n_H = \infty$ (dashed line): (a) shows counter-NB case and (b) co-NB case. Calculation conditions are the same as Fig. 8, except for the magnetic field strength ($B_{ax} = 0.5 \text{ T}$) and the volume averaged beta ($\langle\beta\rangle = 2.7\%$).

HINT code [21, 22]. $B_{ax} = 0.5 \text{ T}$ is almost the same as the magnetic field strength used in the high-beta experiments of the LHD [2]. In $\langle\beta\rangle = 2.7\%$, the magnetic axis is located more torus-outwardly ($R_{ax} \approx 3.9 \text{ m}$). The initial conditions of particles produced by the tangential-NBs and the background plasma are the same as that mentioned in Sec. 3.1. According to the previous study [9], the finite-beta equilibrium magnetic field with $\langle\beta\rangle = 2.7\%$ and $B_{ax} = 0.5 \text{ T}$ has significantly worse properties of high-energy particle confinement compared with the vacuum magnetic field at $B_{ax} = 3 \text{ T}$.

Figure 9 shows $F_\rho(\rho)$ in the finite-beta plasma of the LHD. In Figs. 9(a) and (b), there is a significant difference between $n_H = 0$ and $n_H = \infty$ in $0 < \rho < 1$ as well as $\rho \approx 1$. This result shows that there exit the re-entering particles around the magnetic axis. This is because the particles produced by the tangential-NBs deviate significantly from the flux surface on which its initial point is set in the case of $B_{ax} = 0.5 \text{ T}$.

In the $n_H = 10^{18} \text{ m}^{-3}$ case, clear differences between counter-NB case (Fig. 9(a)) and co-NB case (Fig. 9(b))

can be seen. In co-NB case, the distribution function in $n_H = 10^{18} \text{ m}^{-3}$ is larger than that in $n_H = \infty$ in $0 < \rho < 1$ as well as $\rho \approx 1$. The effect of the re-entering particles on the distribution function is about 5% at $\rho = 0.1$. On the other hand, the distribution function when $n_H = 10^{18} \text{ m}^{-3}$ is almost the same as that when the $n_H = \infty$ in counter-NB case. This result implies that the effect of the charge-exchange loss on the re-entering particles is larger in counter-NB case. This is because the particle produced by counter-NB in torus-outside tends to move in the outer region of the flux surface on which its initial point is set and because their path lengths outside LCFS have a tendency to be longer. These results imply that the charge-exchange loss plays an important role in the confinement of re-entering particles.

The effect of the charge-exchange loss on the distribution function of the high-energy particles depends not only on the neutral density profile but also on the background plasma. We will investigate the effect of the re-entering particles as well as the charge-exchange loss in the distribution function of the NBs with conditions much closer to

those used in the actual LHD experiments.

4. Conclusion

We have developed a new Monte Carlo code based on particle tracing with the use of the real coordinates to trace the re-entering particles properly. The particle loss due to the charge-exchange reaction has been taken into account in this code. This new code has been applied to the analysis of the high-energy particles produced by the tangential-NBs of the LHD. The distribution functions have been investigated in the vacuum magnetic field with $B_{ax} = 3$ T and in the finite-beta plasma ($\langle\beta\rangle = 2.7\%$) with $B_{ax} = 0.5$ T. We have found the following information.

We have confirmed that reasonable distribution functions can be obtained by the code we have developed in the vacuum magnetic field with $B_{ax} = 3$ T. The energy relaxation process of high-energy particles can be analyzed successfully using the developed code, so that reasonable solutions of distribution functions are obtained for particles produced by the tangential-NBs. It is confirmed that the effect of the particle orbit and the charge-exchange loss on the distribution function is properly included.

We have studied the difference in the obtained distribution function caused by the difference in temperature of the back ground plasma in the vacuum magnetic field with $B_{ax} = 3$ T. The shapes of the distribution function in the two temperature cases are found to be almost the same.

We have also investigated the effect of the charge-exchange loss and the re-entering particle on the distribution function in the vacuum magnetic field with $B_{ax} = 3$ T and in the finite-beta plasma with $B_{ax} = 0.5$ T. In the vacuum magnetic field with $B_{ax} = 3$ T, the effect of the re-entering particle is found in the vicinity of the LCFS. On the other hand, the re-entering particles have an effect on the distribution function around the magnetic axis as well as in the vicinity of the LCFS in the finite-beta plasma with $B_{ax} = 0.5$ T. It is also found that the effect of the charge-exchange loss on the distribution function depends on whether the re-entering particles are regarded as lost particles. It is found that it is important to treat the re-

entering particles correctly in the analyses of the distribution function of particles produced by the NBs, particularly in the finite-beta plasma with $B_{ax} = 0.5$ T.

Acknowledgements

We thank Prof. S. Oikawa (Hokkaido University) for fruitful discussions and Dr. M. Osakabe (National Institute for Fusion Science) for giving us information about the LHD NB injector systems. This work is supported by the collaborative research program of NIFS (NIFS08KLHH309) and is partially supported by a Grant-in-Aid for the Scientific Research(B) (18360445) of Japan Society for the Promotion of Science (JSPS).

- [1] A. Iiyosi *et al.*, Nucl. Fusion **39**, 1245 (1999).
- [2] K.Y. Watanabe *et al.*, in Proc. of ITC-17 and ISWS-16 Toki I-13 (2007).
- [3] S. Sudo *et al.*, Nucl. Fusion **30**, 11 (1990).
- [4] T. Yamaguchi *et al.*, Nucl. Fusion **45**, L33 (2005).
- [5] W.A. Cooper *et al.*, Nucl. Fusion **46**, 683 (2006).
- [6] W.A. Cooper *et al.*, Fusion Sci. Technol. **50**, 245 (2006).
- [7] S. Murakami *et al.*, Fusion Sci. Technol. **46**, 241 (2004).
- [8] S. Murakami *et al.*, Nucl. Fusion **46**, S425 (2006).
- [9] R. Seki *et al.*, Plasma Fusion Res. **3**, 016 (2008).
- [10] R.H. Fowler, R.N. Morris, J.A. Rome and K. Hanatani, Nucl. Fusion **30**, 997 (1990).
- [11] K. Hanatani and F. -P. Penningfeld, Nucl. Fusion **32**, 1769 (1992).
- [12] K. Tani *et al.*, J. Phys. Soc. Jpn. **50**, 1726 (1981).
- [13] K. Hamamatsu *et al.*, Plasma Phys. Control. Fusion **49**, 1955 (2007).
- [14] D. Sarafyan, J. Math. Anal. Appl. **40**, 436 (1972).
- [15] T. Watanabe, Trans. Jpn. Soc. Ind. Appl. Mat. **1**, 101 (1991) [in Japanese].
- [16] M.N. Rosenbluth *et al.*, Phys. Rev. **107**, 1 (1957).
- [17] D.J. Huba, 2002 NRL Plasma Formulary 34 (Washington, DC: Naval Research Laboratory).
- [18] R.J. Goldston *et al.*, J. Comput. Phys. **46**, 61 (1981).
- [19] M. Osakabe, private communication.
- [20] J.D. Gaffey, Jr., J. Plasma Phys. **16**, part 2, 149 (1976).
- [21] T. Hayashi, Theory of Fusion Plasmas, EUR 12149 EN 11 (1989).
- [22] K. Harafuji, T. Hayashi and T. Sato, J. Comput. Phys. **81**, 169 (1989).